Fast and Efficient Molecule Detection in Localization-Based Super-Resolution Microscopy by Parallel Adaptive Histogram Equalization

Yiming Li,[†] Yuji Ishitsuka,[†] Per Niklas Hedde,[†] and G. Ulrich Nienhaus[†,‡,§,*]

[†]Institute of Applied Physics and Center for Functional Nanostructures (CFN), Karlsruhe Institute of Technology (KIT), Wolfgang-Gaede-Strasse 1, 76131 Karlsruhe, Germany, [‡]Institute of Toxicology and Genetics, Karlsruhe Institute of Technology (KIT), Hermann-von-Helmholtz-Platz 1, 76344 Eggenstein-Leopoldshafen, Germany, and [§]Department of Physics, University of Illinois at Urbana—Champaign, 1110 West Green Street, Urbana, Illinois 61801, United States

ABSTRACT In localization-based super-resolution microscopy, individual fluorescent markers are stochastically photoactivated and subsequently localized within a series of camera frames, yielding a final image with a resolution far beyond the diffraction limit. Yet, before localization can be performed, the subregions within the frames where the individual molecules are present have to be identified—oftentimes in the presence of high background. In this work, we address the importance of reliable molecule identification for the quality of the final reconstructed super-resolution image. We present a fast and robust algorithm (a-livePALM) that vastly improves the molecule detection efficiency while minimizing false assignments that can lead to image artifacts.

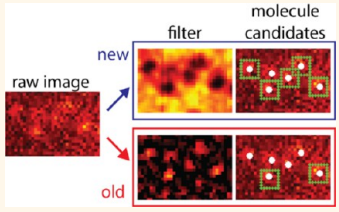

KEYWORDS: super-resolution microscopy · localization microscopy · molecule detection · graphics processing unit (GPU) · recall · precision

Recent advancements in super-resolution fluorescence microscopy have extended the spatial resolution down to tens of nanometers.[1,2] Emergence of these techniques has opened a whole new world of structural detail in microscopic imaging of biological systems. One of the widely used super-resolution microscopy approaches is the stochastic switching method, which includes (fluorescence) photoactivation localization microscopy ((F)PALM)[3,4] and stochastic optical reconstruction microscopy (STORM).[5] This approach relies on fluorophores that can be switched between a fluorescent on- and a nonfluorescent off-state. Unlike standard fluorescence microscopy, which involves excitation of all fluorophores within the field of view, only a few, sparsely distributed molecules are randomly photoactivated to their fluorescent on-state, while leaving the surrounding molecules in the off-state. By repeated image acquisition (10−500 frames/s), up to 10^5 images are collected and subsequently analyzed by specialized software to identify the positions of individual molecules to a precision that markedly exceeds the diffraction limit.

In general, this data analysis can be divided into three steps, (1) molecule detection, where molecule candidates are identified within the raw image; (2) molecule localization, where the identified candidates are analyzed to extract their physical parameters, most importantly, the centers of gravity of their point spread functions (PSFs); and finally (3) image reconstruction, where fitted molecules are plotted as a density map depicting the spatial distribution of all emitters with a resolution in the range of a few tens of nanometers. Recently, much effort has been devoted to improve step 2, the localization of the individual markers, to achieve significant improvements in the precision and speed of the algorithm.[6−10] Once molecules can be precisely localized by these advanced algorithms, the final image quality of the localization-based super-resolution microscopy critically depends on the density of identified molecules. However, far less attention has been paid to improve the initial molecule detection step, perhaps based on the

* Address correspondence to uli@uiuc.edu.

Received for review February 23, 2013 and accepted May 6, 2013.

Published online 10.1021/nn4009388

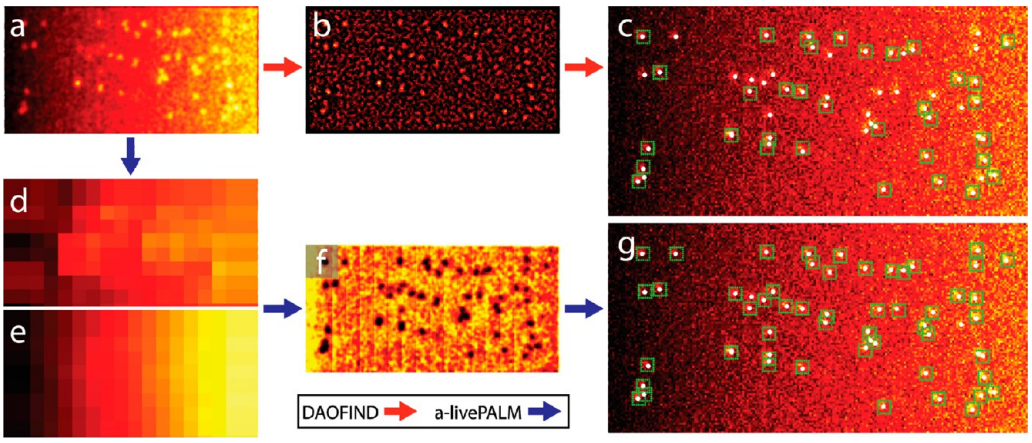

Figure 1. Localization microscopy image processing with the DAOFIND and a-livePALM molecule detection algorithms. The red and blue arrows denote procedures run in DAOFIND and a-livePALM, respectively. In DAOFIND, the raw image is first convoluted with a Gaussian filter (a). The SNRs are calculated (b) and a threshold is set to identify molecule candidates (c). In a-livePALM, the local background parameters (standard deviation (d) and mean (e)) are computed from the raw image (Supporting Information, Figure S1). A *P* value is calculated and mapped for every pixel (f). Molecule candidates are identified as local maxima with the *P* value below the chosen threshold (g).

assumption that falsely identified molecules can be excluded later by multiparameter (total signal counts, width of the point spread function, background, and localization precision) filtering.

Despite smaller attention among the super-resolution community, the molecule detection step has been extensively studied among the broader image-processing field.[11,12] The performance of any detection algorithm critically depends on the signal-to-noise ratio (SNR)[13] and the signal-to-background ratio (SBR).[14] Typically, a molecule detection algorithm utilizes a single set of initial parameters, such as intensity count and SNR, for thresholding. However, setting the proper thresholds for signal detection is a major challenge in working with biological samples because both SNR and SBR may fluctuate over time and even within the same imaging area. This temporal and spatial heterogeneity in the SNR and SBR distributions may arise from the inherent nature of the biological sample, photobleaching of the fluorophores, or from common technical issues such as changes in the laser intensity and uneven sample illumination. Improper thresholding can result in either missing valid molecules or mistaking noise for real molecules. Consequently, there is a clear need to develop a more robust approach to setting a threshold for molecule detection.

In this paper, we present a fast and robust molecule detection algorithm that utilizes parallel application of adaptive histogram equalization[15] to identify molecule candidates even in the presence of heterogeneous background. We evaluated the performance of our new algorithm and compared the results to the search algorithm widely used in localization microscopy on both simulated and experimental data. We found that our new algorithm can identify molecule candidates with higher efficiency and reliability over a wide range of background conditions.

RESULTS AND DISCUSSION

Although there are many (F)PALM/STORM analysis programs available, most of them utilize the "DAOFIND" algorithm for molecule detection.[3,5,9,16–19] The schematic of the analysis steps of our new algorithm, accurate livePALM (a-livePALM), and the DAOFIND algorithm are shown in Figure 1. In both approaches, the raw image (Supporting Information, Figure S1) is first convoluted by a Gaussian kernel to reduce noise and to enhance the signal (Figure 1a). DAOFIND directly identifies molecule candidates in the convoluted image by setting a threshold based on the SNR (Figure 1b). Instead of setting a threshold to the SNR, a-livePALM performs additional local contrast enhancements by the adaptive histogram equalization technique. In practice, we calculate a *P* value (P = 1 − normal cumulative distribution function (CDF)) for each pixel using the standard deviation (Figure 1d) and the mean background of its surrounding region (Figure 1e). The *P* value (Figure 1f) represents the probability of the pixel to be part of the surrounding background. Local maxima with a *P* value below the threshold (P = 0.08, see Methods section) are assigned to molecule candidates (Figure 1g). Squares and white dots in Figure 1c and g represent coordinates of molecule candidates identified by the algorithm and the actual coordinates of simulated molecules, respectively.

The advantage of this approach is that the *P* value is insensitive to changes of the SNR and the SBR, and significantly enhances signal contrast with minimal distortion of the image. To show the difference of the signal enhancement methods used by DAOFIND and a-livePALM, we generated an image of five molecules placed over a linearly increasing background and processed it by DAOFIND and a-livePALM (Figure 2). The intensity profile of the molecules in the absence of

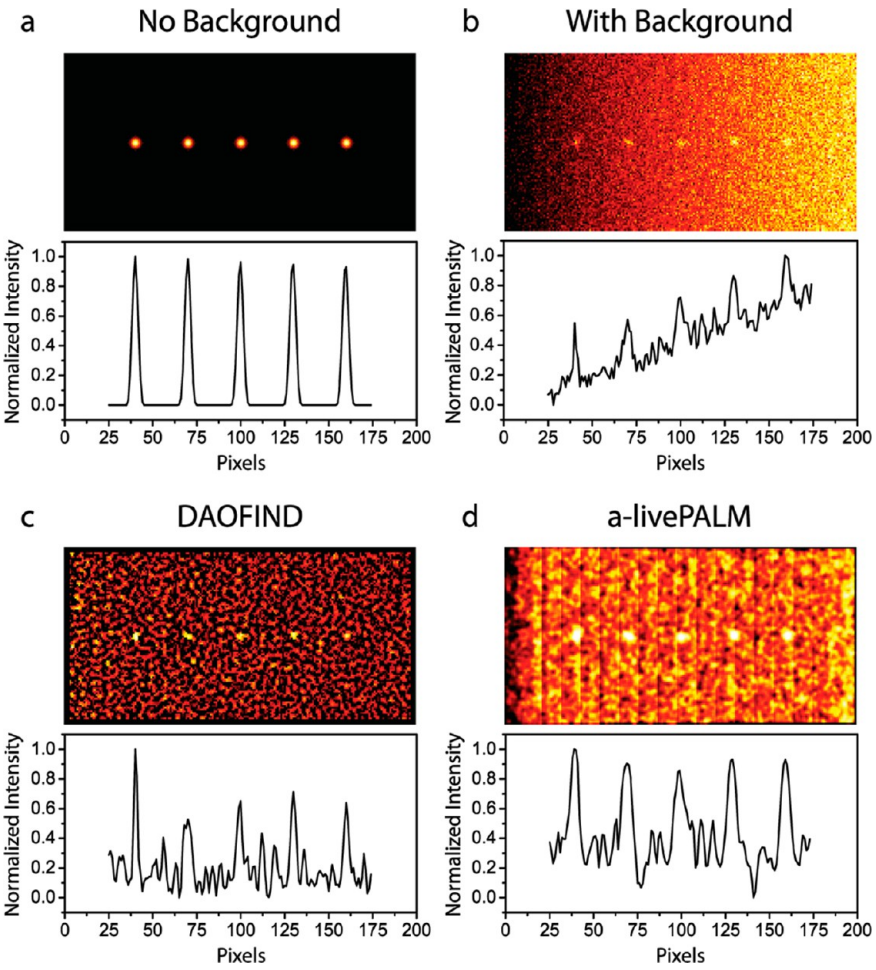

Figure 2. (a) Simulated image of five molecules without background (top). This intensity profile (bottom) serves as a reference. (b) Image after adding a linearly increasing background and Poisson noise (top) and its intensity profile (bottom). (c) SNR map of DAOFIND (top) and its intensity profile (bottom). (d) *P* value map of a-livePALM algorithm (top) and its intensity profile (bottom). The color scale of the *P* value map (d, top) has been inverted to enable a comparison with the other maps.

noise is shown in Figure 2a as a reference. By adding linearly increasing background and Poisson noise, a significant decrease of contrast is generated in the intensity profile (Figure 2b). The DAOFIND algorithm takes the Gaussian-convoluted image from Figure 2b and generates the SNR map for each pixel. A top-hat filter with grayscale opening was used to generate the SNR map (Figure 2c). The intensity profile shows an overall flattening of the background. However, background features are also enhanced in a way that resembles signals from actual molecules. This could lead to registration of false positive molecules. For comparison, the *P* value map from the a-livePALM adaptive histogram equalization algorithm and its corresponding intensity profile are shown in Figure 2d. The contrast of the molecule signal is evenly enhanced over the entire image, and the intensity profile is easily distinguishable from the background.

To assess the efficiency and accuracy of molecule detection, we compared a-livePALM against our previously published algorithm, livePALM,[20] and several publicly available fast programs: QuickPALM,[16] MaLiang,[9] and rapidSTORM.[21] Two parameters, recall and precision, are employed to evaluate the performance of the search algorithm. Recall is defined as the ratio of the number of true positive molecules to the total number of simulated molecules. A true positive molecule is a molecule with a returned coordinate within a certain distance (*D*) of the actual coordinate. Molecules outside of *D* are classified as false positive molecules. Precision is defined as the ratio of the number of true positive molecules to the number of all detected molecules (*i.e.*, true + false). We simulated 1000 images (100 × 200 pixels) with molecules randomly placed over a linearly increasing background (Supporting Information, Figure S1). These simulations were performed for varying molecule densities (0.1−1 molecule/μm^2). To account for the fact that the different algorithms compared in this work use different molecule localization methods, we chose a rather large value of 1.5 pixels for *D* to minimize the influence of this variable on recall and precision (Supporting Information, Figure S2). Recall and precision results are

plotted as a function of molecule density (Figure 3a,b). Different sets of parameters were tested for the three publicly available programs to optimize their performances (Supporting Information, Figure S3); selected parameters used for the performance evaluation on our data are shown in Supporting Information, Figure S4–S6. In general, except for rapidSTORM, the precision was high over the entire range of the molecule density, while the recall generally decreased with increasing density. Among the programs evaluated, our new algorithm, a-livePALM, showed the highest efficiency (recall) of identifying molecule candidates while maintaining a high precision.

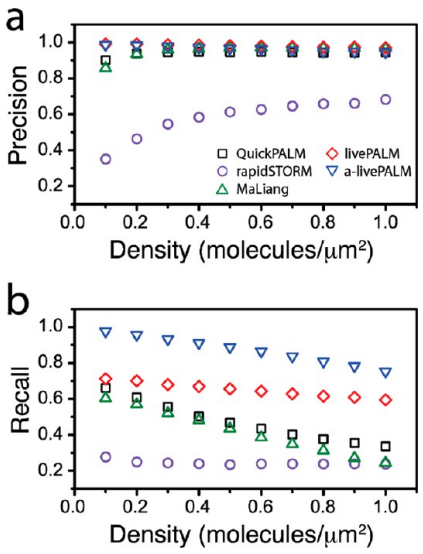

Figure 3. Performance assessment of various image reconstruction algorithms (QuickPALM, RapidSTORM, MaLiang, livePALM, and a-livePALM). By using a set of simulated data images with varying molecule densities, the performances were evaluated by analyzing the (a) precision and (b) recall parameters.

To directly quantify the molecule detection performance of the algorithm, we tested two of the best algorithms from the first evaluation, livePALM and a-livePALM, on a different set of simulated molecules (intensity, I_0, of 150, 200, or 250 photons) that are well separated from each other, placed over a range of background conditions (Gaussian noise, $N_{i,j}(\delta)$, and background (BG) level, N_{bg}, see Methods) within the same image. A sample image is shown in Supporting Information, Figure S7. To obtain a meaningful comparison between livePALM and a-livePALM, we used the same molecule localization algorithm, the maximum likelihood estimation method.[10] We conducted the molecule search on simulated images using two different thresholding methods for livePALM. The search parameters (low photon threshold and SNR) of livePALM were adjusted either for high precision (precision > 0.90 for over 50% of molecules, precision optimized, PO, Figure 4b,e) or for high recall efficiency (maximum recall, recall optimized, RO, Figure 4c,f). a-livePALM (Figure 4d) and livePALM PO (Figure 4e) showed a comparable result for the precision, but a markedly lower recall for livePALM PO as the background level increased (compare Figure 4a and b). The recall also deteriorated as the number of photons decreased and Gaussian noise increased. For livePALM, the recall of molecules with only 150 detected photons is low, especially with high background. The precision values computed from these few molecules are more

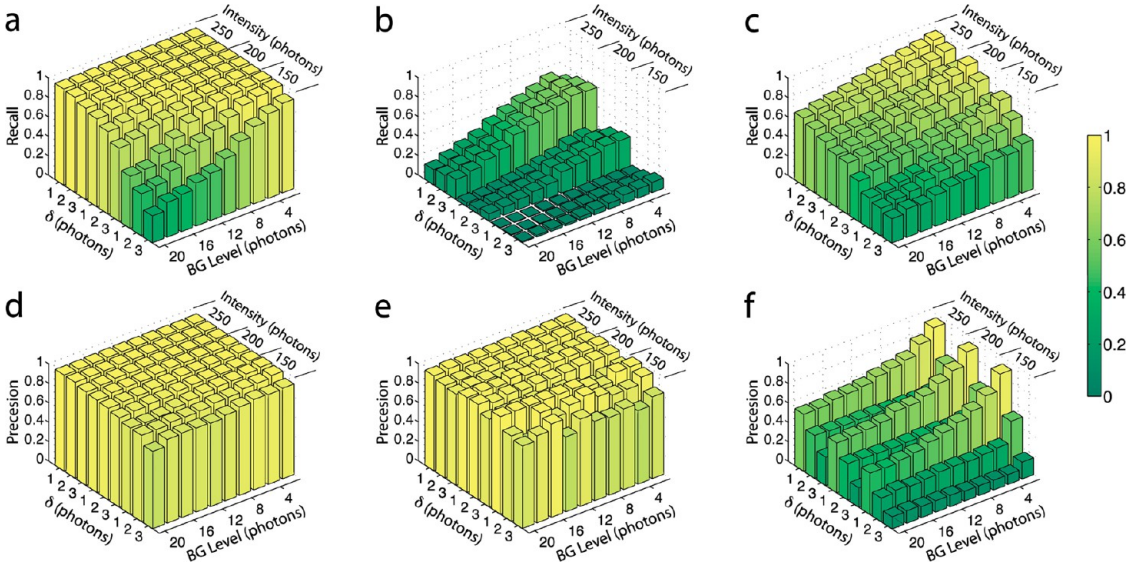

Figure 4. Recall and precision performances of the a-livePALM and livePALM programs. Three different sets of simulated images (intensity of 150, 200, or 250 photons/molecule), synthesized with different background (BG) levels (2–20 photons) and standard deviation (δ) of added Gaussian noise (1, 2, or 3 photons) were analyzed. The molecule detection performance evaluated by recall and precision values from a-livePALM (a, d), livePALM with PO threshold condition (b,e) and livePALM with RO threshold condition (c,f) are shown.

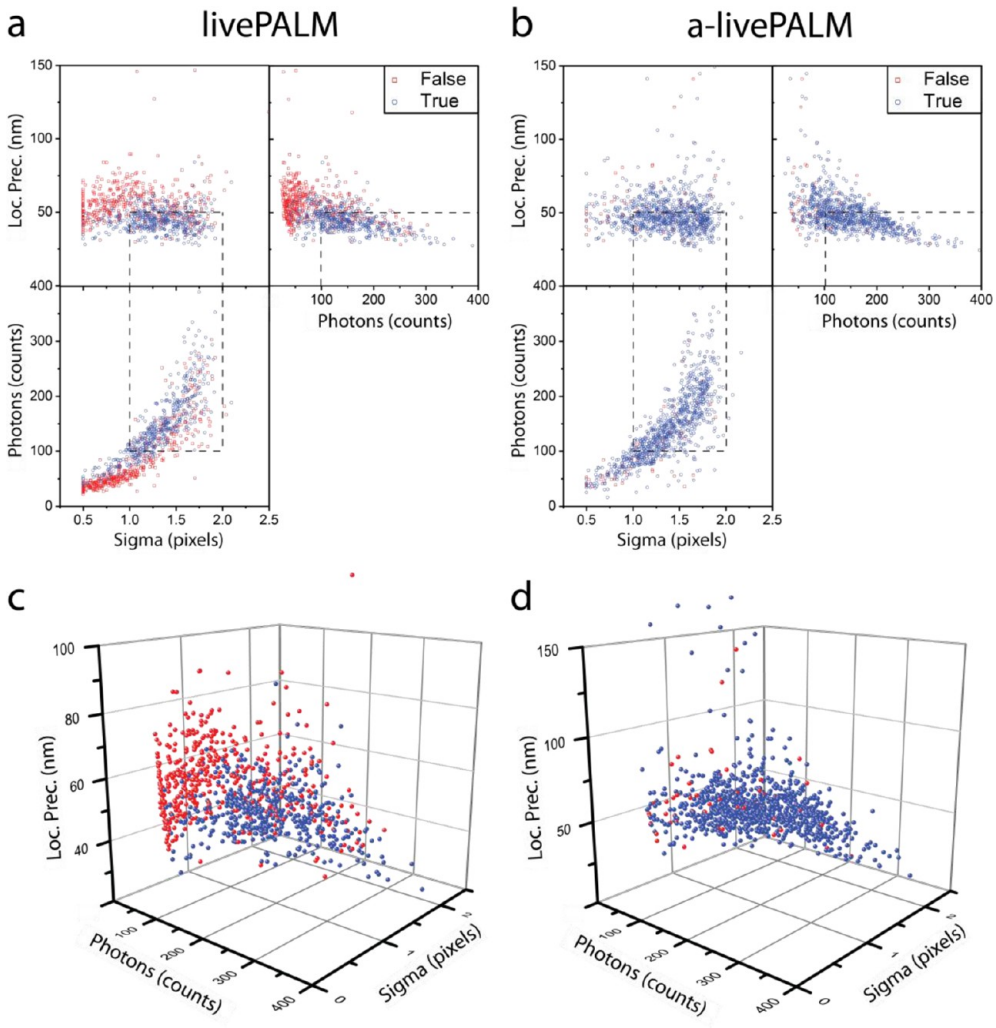

Figure 5. 2D/3D plots of fitted parameters (photon counts, localization precision, and sigma) from livePALM (RO) and a-livePALM on simulated data (Supporting Information, Figure S7). 2D plots of fitted parameters of (a) livePALM and (b) a-livePALM are shown. The data were filtered with 100−500 photons, <50 nm localization precision, and 1−2 pixels sigma (shown by dotted lines). The corresponding 3D plots of panels (a) and (b) are shown in panels (c) and (d). Red and blue dots represent false positive and true positive molecules, respectively.

prone to fluctuations and could result in nonincremental changes in the precision over varying BG levels (Figure 4e). a-livePALM showed a high level of recall for the entire range of imaging conditions. In real experiments, the recall parameter should be maximized to improve the final image quality of the biological structure of interest. The recall can be improved by using the livePALM RO condition (Figure 4c), however, only at the expense of its precision performance (Figure 4f). These comparisons demonstrate the overall high efficiency and reliability of a-livePALM over wide ranges of SNR and SBR while using only a single thresholding parameter.

The overall precision of the coarsely selected molecule data set can still be improved if false positive molecules can be removed efficiently by filtering. To this end, we took the data set which yielded ~50% precision from livePALM analysis and plotted the distributions of the number of photons, background, the width of the point spread function, and the localization precision, of true and false positive molecules in Supporting Information, Figure S8 and 2D/3D plots of fitted parameters in Figure 5. Two example images of true and false positive molecules are shown in Supporting Information, Figure S9. Multiparameter filtering revealed that, due to considerable overlap in the parameter distributions of true and false positive molecules, a significant fraction (~20%) of false positive molecules could not be eliminated from the data (Supporting Information, Table S1). By contrast, a-livePALM yields a final false positive population of merely 1% on the same data set. These results underscore the importance of properly identifying molecules from the raw images in the first place and not relying on postfiltering.

As the image reconstruction is based on processing thousands of image frames, it is of utmost importance that the analysis algorithm can run at high speed to

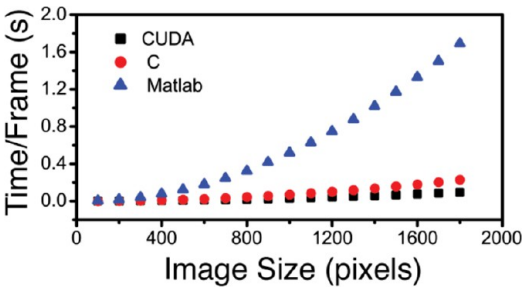

Figure 6. Processing speed of the a-livePALM algorithm implemented in Matlab, C, and CUDA (GPU processing).

keep up with image acquisition. Early versions of image reconstruction software for localization-based super-resolution microscopy were laborious and took many hours until completion, so that acquisition parameters (laser intensity, acquisition time, *etc.*) were difficult to adjust during the experiment. As mentioned above, numerous algorithms have been developed to accelerate image reconstruction, however, mostly in the molecule localization step.[9,10,16,18,20] This is primarily because relatively simple, hence fast, algorithms have been used for the molecule detection step. In the broader image-processing field, various highly sophisticated denoising techniques are known that can deal with images with varying background.[11,12] Naturally, advanced molecule detection algorithms come at the expense of added computational complexity. To avoid slowing of the analysis while maintaining performance, we have coded our algorithm so that it utilizes the parallel processing power of GPUs for the molecule detection step. As a result, our software achieves a processing speed comparable to state-of-art fast software even with the additional background estimation (Figure 6 and Supporting Information, Figure S10).

Comparison of livePALM and a-livePALM on experimental data further highlights the strengths of our new method. Figure 7 shows PALM images reconstructed from 1600 frames of raw data of the fusion protein RITA-mcavRFP[22] in live HeLa cells analyzed by livePALM RO and a-livePALM. The raw wide field image shows considerable SNR heterogeneity within the image (Supporting Information, Figure S11). The overall fluorescence intensity varied in time due to power adjustment of the 405-nm laser and photobleaching of the molecules (Supporting Information, Figure S12). We found a significantly higher molecule detection efficiency using our new algorithm, in agreement with our findings on simulated data. We plotted these molecules with the same brightness and contrast setting for a direct comparison (Figure 7a–d). A total of 273 751 and 474 385 molecules were identified by livePALM RO and a-livePALM, respectively (Figure 7e), whereas livePALM PO detected only 98 013 molecules (Supporting Information, Figure S13). In regions with high SNR, livePALM performed equally well as

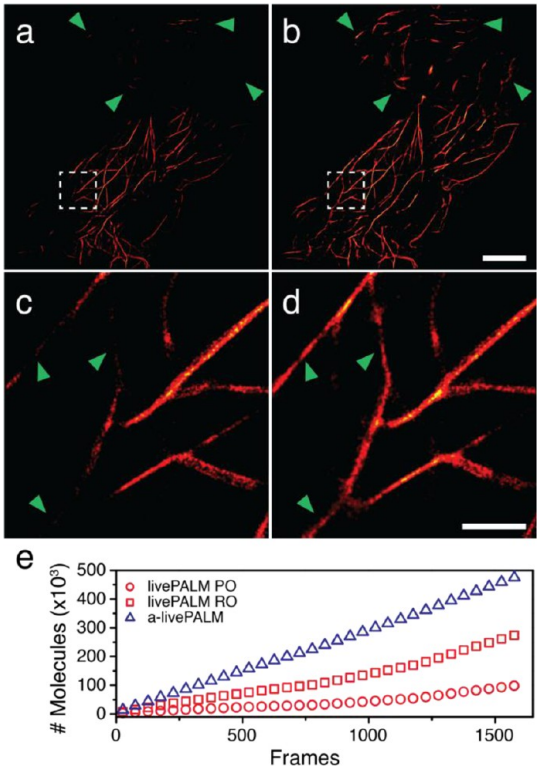

Figure 7. Performance of livePALM and a-livePALM molecule detection algorithms applied to experimental data. PALM images of microtubules in live HeLa cells, labeled with the fusion protein RITA-mcavRFP, were reconstructed by using (a,c) the livePALM RO and (b,d) a-livePALM algorithms. Arrows indicate structures reconstructed by a-livePALM, but missed by livePALM. Scale bars, 5 μm (a,b) and 1 μm (c,d). (e) Accumulated number of molecules identified by livePALM PO, livePALM RO, and a-livePALM upon processing 1600 image frames.

a-livePALM. In regions with lower SNR, livePALM performed poorly, as already seen with simulated images (Figure 4). As a result, some structures were missing from the image (indicated by arrows). In particular, for livePALM, the microtubules located in the upper third of the reconstructed image are missing due to the high background level (Supporting Information, Figure S11).

CONCLUSIONS

Our new molecule detection algorithm is capable of identifying molecules in (F)PALM/STORM images with high efficiency and reliability even in the presence of widely varying background. These improvements yield an enhanced reliability in quantitative data analysis and higher resolution in the final reconstructed images. The significantly improved detection yield and reliability will benefit experiments that require a fast time resolution as well as more accurate quantification of molecules.[23–26] Our algorithm will also become useful for multicolor super-resolution imaging using fluorescent protein markers, where the signal of fluorophores may be considerably compromised by

the autofluorescence from the cell. Although we have limited ourselves to single peak fitting of the identified molecules in 2D imaging in this work, our search algorithm is directly applicable to multipeak fitting methods as well as 3D imaging methods that have been introduced in recent years.[17,27,28]

METHODS

Microscopy. HeLa cells were transiently transfected with a RITA-mcavRFP fusion construct, a tubulin binding protein fused with a photoconvertible version of the red fluorescent protein.[22] PALM image acquisition was performed at room temperature (24 °C) on a modified inverted microscope (Axiovert 200, Zeiss, Jena, Germany) equipped with a high NA oil immersion objective (60×, 1.45-NA oil immersion, Olympus, Hamburg, Germany). We employed three diode-pumped solid-state lasers, with wavelengths 561 nm (GCL-150-561, Crysta-Laser, Reno, NV), 473 nm (LSR473-200-T00, Laserlight, Berlin, Germany) and 405 nm (CLAS^{II} 405-50, Blue Sky Research, Milpitas, CA) for excitation and photoactivation of the fluorophores. The laser sources were combined *via* appropriate dichroic mirrors (AHF, Tübingen, Germany) and guided through an AOTF (AOTFnC-400.650, A-A, Opto-Electronic, Orsay Cedex, France) to control the laser intensities at the sample prior to coupling into a single mode fiber (OZ Optics, Ottawa, Ontario, Canada). The fluorescent proteins were converted from their green to their red emitting forms using 405-nm light of low intensity (0−10 W/cm^2) and subsequently imaged by 561-nm illumination (200−400 W/cm^2) with an EMCCD camera (Ixon DV887ECS-BV, Andor, Belfast, Northern Ireland) at 100 ms time resolution. After passing the excitation dichroic (z 405/473/561, AHF, Tübingen, Germany), fluorescence emission was filtered by a bandpass filter (617/73).

Image Simulation. To evaluate the performance of super-resolution algorithms, synthesized test images are routinely used.[13,14] We have examined the performance of our search algorithm with simulated single fluorescence emitters with varying SNR and background. All simulated images were generated by using MATLAB.

Considering the finite pixel size, the final simulated signal is given by

$$F_{i,j} = \mathrm{Pois}(I_0 \int_A \mathrm{PSF}(u, v)\, du\, dv + \mathrm{bg}_{i,j}) \quad (1)$$

Here, Pois(x) is a Poissonian random number with a mean value of x. I_0 is the number of photons registered for a given fluorophore. The integral extends over the area of each pixel, A. The point spread function, PSF(x, y), is approximated by a two-dimensional Gaussian function,

$$\mathrm{PSF}(x, y) = \frac{1}{2\pi\sigma^2} \exp(\frac{(x - x_0)^2 + (y - y_0)^2}{2\sigma^2}) \quad (2)$$

where (x_0, y_0) is the position of the emitter. The background level of each pixel (*e.g.*, from diffusing impurity molecules or thermal noise),

$$\mathrm{bg}_{i,j} = N_{\mathrm{bg}} + N_{i,j}(\delta) \quad (3)$$

is modeled by a constant background or a linearly increasing background, N_{bg}, and is additionally varied by Gaussian noise, $N_{i,j}(\delta)$, with standard deviation, δ.

Molecules with different SNR and SBR were synthesized within the same image to model heterogeneous background (Supporting Information, Figures S1 and S7). For the nonoverlapping molecules in Figure S7, each molecule was randomly plotted in the center (10 × 10 pixels) of a block (30 × 30 pixels). Three types of molecules (I_0 = 150, 200, or 250 photons) were used for the evaluation. For each molecule, the background level (N_{bg}) was varied from 2 to 20 photons with the standard deviation of the additional Gaussian noise, δ, of 1, 2, or 3 photons. The resulting SNR of the final image ranged from 1.3 to 3.3; the SBR ranged from 0.4 to 6.8. We note that the SNR of a molecule is defined by SNR = (I − bg)/σ,[29] where I and bg are the maximum intensities of the single molecule signal and the background, respectively; σ is the standard deviation of the background.

Description of the Algorithms for Data Processing. Identification of molecule candidates involves three steps within our new algorithm: noise reduction, local background estimation, and selection of appropriate local maxima according to the local background condition. The general outline of this process is shown in Figure 1. For noise reduction, we convoluted the raw images with a Gaussian kernel,[13] with a standard deviation, σ, depending on the data set. Typically, we used σ = 1 pixel for 2D localization images. To estimate the local background, each image is first subdivided into small local areas (11 × 11 pixels). The background of each local area is quantified by the mean value and the standard deviation of its larger surrounding area (31 × 31 pixels) to improve the sampling. Using the local mean background and standard deviation, the P value of each pixel value is calculated. Only pixels with a P value above a user-defined threshold are selected, and local maxima (within 7 × 7 pixels) among these pixels are identified as molecule candidates. Small subimages (7 × 7 pixels) around these local maxima are extracted for single molecule localization. For pixels on the boundaries, which are not surrounded by a 31 × 31 pixels area for background calculation, the background parameters were transferred from the nearest nonboundary pixels. Different P values were tested for the synthesized data (Supporting Information, Figure S14). A P value of 0.08 produced optimal results for identifying molecules. Lower P values yield high precisions, but lower recalls. By contrast, a high P value yields a high recall, but a lower precision. In the experimental setting, one can find an appropriate P value by minimizing the number of molecules identified from areas void of fluorescent molecules (*e.g.*, areas where there are no cells).

For the subsequent single molecule localization step, a two-dimensional Gaussian (plus a constant background) model is fitted to the molecule candidates isolated from the raw data. Various algorithms have been suggested to localize single molecules. Least squares fitting,[30] maximum likelihood estimation,[31] the fluoroBancroft algorithm,[6] and the wavelet analysis[32] are common approaches. Among these, we use Gaussian fitting with the recently developed GPU-based maximum likelihood estimator (MLE) algorithm.[10] This technique achieves theoretically minimum uncertainty (Crámer-Rao lower bound, CRLB) while vastly speeding up the single molecule localization process.

The final super-resolution image is reconstructed from the coordinates of the localized molecules. Molecules that appear in n successive frames and are spatially close (<100 nm) are considered to be identical. In the final super-resolution image, the molecule is plotted n times with the weighted value of 1/n so that the intensity of the reconstructed image represents the real density of molecules.

Software and Hardware Implementation. The data processing procedures were run in MATLAB R2010b (The Mathworks, USA) environment. The workflow of the program is shown in Supporting Information, Figure S15. Both the CPU based C-code (green boxes) and the GPU based C-code (red boxes, Nvidia CUDA, http://www.nvidia.com/object/cuda_home.html) are compiled to MATLAB mex files. The local background estimation (CPU) and the Gaussian noise filtering of the image (GPU) are run in parallel since those computations are totally independent of each other. On the basis of the background parameters and the denoised image, the normal CDF of each pixel is calculated in the GPU. Those pixels with P values below a certain threshold are selected, and the local maxima among these pixels are determined as molecule candidates. The arrays around the candidates are extracted and finally

passed into the GPU global device memory for single molecule localization.

The software was run on a personal computer with an Intel(R) Core i7-2600 processor clocked at 3.40 GHz and 8.0 GB memory. A NVIDIA GeForce GTX 560Ti graphics card with 1.0 GB memory was used for GPU based computation. For a typical image size of 512 × 512 pixels, acquired by the camera, the processing time is 15−30 ms per image, depending on its complexity. The speed is comparable to the maximum full frame rate of current EMCCD cameras and, therefore, allows real-time data processing.

Conflict of Interest: The authors declare no competing financial interest.

Acknowledgment. We thank B. Rieger (Delft University of Technology, The Netherlands) for making his GPU-based single molecule localization program available for us. This work was supported by the state of Baden-Württemberg and the Deutsche Forschungsgemeinschaft (DFG) through the Center for Functional Nanostructures (CFN) and the Karlsruhe School of Optics and Photonics (KSOP).

Supporting Information Available: Simulated raw images, input parameters of three fast PALM/STORM programs, and additional performance data and image reconstruction results. This material is available free of charge *via* the Internet at http://pubs.acs.org.

REFERENCES AND NOTES

1. Hell, S. W. Far-Field Optical Nanoscopy. *Science* **2007**, *316*, 1153–1158.
2. Huang, B.; Babcock, H.; Zhuang, X. Breaking the Diffraction Barrier: Super-Resolution Imaging of Cells. *Cell* **2010**, *143*, 1047–1058.
3. Betzig, E.; Patterson, G. H.; Sougrat, R.; Lindwasser, O. W.; Olenych, S.; Bonifacino, J. S.; Davidson, M. W.; Lippincott-Schwartz, J.; Hess, H. F. Imaging Intracellular Fluorescent Proteins at Nanometer Resolution. *Science* **2006**, *313*, 1642–1645.
4. Hess, S. T.; Girirajan, T. P. K.; Mason, M. D. Ultra-High Resolution Imaging by Fluorescence Photoactivation Localization Microscopy. *Biophys. J.* **2006**, *91*, 4258–4272.
5. Rust, M. J.; Bates, M.; Zhuang, X. Sub-Diffraction-Limit Imaging by Stochastic Optical Reconstruction Microscopy (STORM). *Nat. Methods* **2006**, *3*, 793–795.
6. Andersson, S. B. Localization of a Fluorescent Source without Numerical Fitting. *Opt. Express* **2008**, *16*, 18714–18724.
7. Ma, H.; Long, F.; Zeng, S.; Huang, Z.-L. Fast and Precise Algorithm Based on Maximum Radial Symmetry for Single Molecule Localization. *Opt. Lett.* **2012**, *37*, 2481–2483.
8. Parthasarathy, R. Rapid, Accurate Particle Tracking by Calculation of Radial Symmetry Centers. *Nat. Methods* **2012**, *9*, 724–726.
9. Quan, T. W.; Li, P.; Long, F.; Zeng, S.; Luo, Q.; Hedde, P. N.; Nienhaus, G. U.; Huang, Z. L. Ultra-Fast, High-Precision Image Analysis for Localization-Based Super Resolution Microscopy. *Opt. Express* **2010**, *18*, 11867–11876.
10. Smith, C. S.; Joseph, N.; Rieger, B.; Lidke, K. A. Fast, Single-Molecule Localization that Achieves Theoretically Minimum Uncertainty. *Nat. Methods* **2010**, *7*, 373–375.
11. Ruusuvuori, P.; Tarmo, A.; Sharif, C.; Cecilia, G. T.; Jyrki, S.; Mirko, B.; Aimée, D.; Lucas, P.; Oli, Y. H. Evaluation of Methods for Detection of Fluorescence Labeled Subcellular Objects in Microscope Images. *BMC Bioinformatics* **2010**, *11*, 248.
12. Smal, I.; Loog, M.; Niessen, W.; Meijering, E. Quantitative Comparison of Spot Detection Methods in Fluorescence Microscopy. *IEEE Trans. Med. Imag.* **2010**, *29*, 282–301.
13. Křížek, P.; Raška, I.; Hagen, G. M. Minimizing Detection Errors in Single Molecule Localization Microscopy. *Opt. Express* **2011**, *19*, 3226–3235.
14. Quan, T. W.; Zhu, H. Y.; Liu, X. M.; Liu, Y. F.; Ding, J. P.; Zeng, S. Q.; Huang, Z. L. High-Density Localization of Active Molecules Using Structured Sparse Model and Bayesian Information Criterion. *Opt. Express* **2011**, *19*, 16963–16974.
15. Pizer, S. M.; Amburn, E. P.; Austin, J. D.; Cromartie, R.; Geselowitz, A.; Greer, T.; Terhaarromeny, B.; Zimmerman, J. B.; Zuiderveld, K. Adaptive Histogram Equalization and Its Variations. *Comput. Vision Graph.* **1987**, *39*, 355–368.
16. Henriques, R.; Lelek, M.; Fornasiero, E. F.; Valtorta, F.; Zimmer, C.; Mhlanga, M. M. QuickPALM: 3D Real-Time Photoactivation Nanoscopy Image Processing in ImageJ. *Nat. Methods* **2010**, *7*, 339–340.
17. Holden, S. J.; Uphoff, S.; Kapanidis, A. N. DAOSTORM: an Algorithm for High- Density Super-Resolution Microscopy. *Nat. Methods* **2011**, *8*, 279–280.
18. Wolter, S.; Schuttpelz, M.; Tscherepanow, M.; Van De Linde, S.; Heilemann, M.; Sauer, M. Real-Time Computation of Subdiffraction-Resolution Fluorescence Images. *J. Microsc.* **2010**, *237*, 12–22.
19. York, A. G.; Ghitani, A.; Vaziri, A.; Davidson, M. W.; Shroff, H. Confined Activation and Subdiffractive Localization Enables Whole-Cell PALM with Genetically Expressed Probes. *Nat. Methods* **2011**, *8*, 327–333.
20. Hedde, P. N.; Fuchs, J.; Oswald, F.; Wiedenmann, J.; Nienhaus, G. U. Online Image Analysis Software for Photoactivation Localization Microscopy. *Nat. Methods* **2009**, *6*, 689–690.
21. Wolter, S.; Sauer, M. Follow-up to paper by S. Wolter, M. Schüttpelz, M. Tscherepanow, S. van de Linde, M. Heilemann, and M. Sauer Entitled Real-Time Computation of Subdiffraction-Resolution Fluorescence Images. *J. Microsc.* **2012**, *245*, 109.
22. Wacker, S. A.; Alvarado, C.; von Wichert, G.; Knippschild, U.; Wiedenmann, J.; Clauss, K.; Nienhaus, G. U.; Hameister, H.; Baumann, B.; Borggrefe, T.; *et al.* RITA, a Novel Modulator of Notch Signalling, Acts *via* Nuclear Export of RBP-J. *EMBO J.* **2011**, *30*, 43–56.
23. Sengupta, P.; Jovanovic-Talisman, T.; Skoko, D.; Renz, M.; Veatch, S.; Lippincott-Schwartz, J. Probing Protein Heterogeneity in the Plasma Membrane Using PALM and Pair Correlation Analysis. *Nat. Methods* **2011**, *8*, 969–975.
24. Lee, S. H.; Shin, J. Y.; Lee, A.; Bustamante, C. Counting Single Photoactivatable Fluorescent Molecules by Photoactivated Localization Microscopy (PALM). *Proc. Natl. Acad. Sci. U.S.A.* **2012**, *109*, 17436–17441.
25. Annibale, P.; Vanni, S.; Scarselli, M.; Rothlisberger, U.; Radenovic, A. Quantitative Photo Activated Localization Microscopy: Unraveling the Effects of Photoblinking. *PLoS ONE* **2011**, *6*, e22678.
26. Gunzenhauser, J.; Olivier, N.; Pengo, T.; Manley, S. Quantitative Super-Resolution Imaging Reveals Protein Stoichiometry and Nanoscale Morphology of Assembling HIV-Gag Virions. *Nano Lett.* **2012**, *12*, 4705–4710.
27. Huang, F.; Schwartz, S. L.; Byars, J. M.; Lidke, K. A. Simultaneous Multiple-Emitter Fitting for Single Molecule Super-Resolution Imaging. *Biomed. Opt. Express* **2011**, *2*, 1377–1393.
28. Wang, Y.; Quan, T.; Zeng, S.; Huang, Z.-L. PALMER: a Method Capable of Parallel Localization of Multiple Emitters for High-Density Localization Microscopy. *Opt. Express* **2012**, *20*, 16039–16049.
29. Cheezum, M. K.; Walker, W. F.; Guilford, W. H. Quantitative Comparison of Algorithms for Tracking Single Fluorescent Particles. *Biophys. J.* **2001**, *81*, 2378–2388.
30. Thompson, R. E.; Larson, D. R.; Webb, W. W. Precise Nanometer Localization Analysis for Individual Fluorescent Probes. *Biophys. J.* **2002**, *82*, 2775–2783.
31. Ober, R. J.; Ram, S.; Ward, E. S. Localization Accuracy in Single-Molecule Microscopy. *Biophys. J.* **2004**, *86*, 1185–1200.
32. Izeddin, I.; Boulanger, J.; Racine, V.; Specht, C. G.; Kechkar, A.; Nair, D.; Triller, A.; Choquet, D.; Dahan, M.; Sibarita, J. B. Wavelet Analysis for Single Molecule Localization Microscopy. *Opt. Express* **2012**, *20*, 2081–2095.